

A boundary layer framework considering material gradation effects

Do-Jun Shim, Glaucio H. Paulino ^{*}, Robert H. Dodds Jr.

*Department of Civil and Environmental Engineering, University of Illinois at Urbana-Champaign,
Newmark Laboratory, 205 North Mathews Avenue, Urbana, IL 61801, USA*

Received 10 March 2005; received in revised form 30 August 2005; accepted 23 September 2005
Available online 28 November 2005

Abstract

This paper describes the development and application of a novel modified boundary layer (MBL) model for graded nonhomogeneous materials, e.g. functionally graded materials (FGMs). The proposed model is based on a middle-crack tension, $M(T)$, specimen with traction boundary conditions applied to the top and lateral edges of the model. Finite element analyses are performed using WARP3D, a fracture mechanics research finite element code, which incorporates elements with graded elastic and plastic properties. Elastic crack-tip fields obtained from the proposed MBL model show excellent agreement with those obtained from full models of the cracked component for homogeneous and graded nonhomogeneous materials. The K – T dominance of FGMs is investigated by comparing the actual stress fields with the asymptotic stress fields (the Williams' solution). The examples investigated in the present study consider a crack parallel to the material gradient. Results of the present study provide insight into the K – T dominance of FGMs and also show the range of applicability of the proposed MBL model. The MBL model is applied to analyze the elastic–plastic crack-tip response of a Ti/TiB FGM SE(T) specimen. The numerical results demonstrate that the proposed MBL model captures the effect of T -stress on plastic zone size and shape, constraint effects, etc. for such configurations.

© 2005 Elsevier Ltd. All rights reserved.

Keywords: Functionally graded material (FGM); Modified boundary layer model; K – T dominance; 3-D finite element analysis; Graded element

1. Introduction

The modified boundary layer (MBL) formulation has been adopted by many researchers to analyze the elastic–plastic crack-tip fields in homogeneous materials [1–4]. The “standard” MBL model consists of a disk-shaped mesh that represents a single-ended crack in an infinite body. The model is loaded by remote boundary conditions applied as tractions or equivalent displacements given by the first two terms (K and T) of the Williams' [5] solution. This model simulates the crack-tip conditions in an arbitrary geometry, provided that the plasticity remains well contained within the body, i.e. small-scale yielding (SSY) conditions

^{*} Corresponding author. Tel.: +1 217 333 3817; fax: +1 217 265 8041.
E-mail address: paulino@uiuc.edu (G.H. Paulino).

prevail. The MBL model has been employed to investigate the effect of T -stress on the elastic–plastic crack-tip fields [1,2], to characterize constraint effects [3], to study ductile crack growth [4], and to many other fracture mechanics problems that consider homogeneous material properties.

Despite its potential usefulness, the “standard” MBL formulation for graded nonhomogeneous materials, e.g. functionally graded materials (FGMs), has not yet been developed. For graded nonhomogeneous materials, a new degree of freedom, i.e. the intrinsic length scale of the material, must be reflected in the MBL formulation. The material length scale invalidates the use of the “standard” MBL formulation, i.e. the disk-shaped model most often adopted for homogeneous materials. In this sense, a new boundary layer formulation applicable for graded nonhomogeneous materials is needed. Such boundary layer formulation is especially needed to simplify the elastic–plastic analysis of, for example, a three dimensional (3-D) surface crack in FGMs. K and T values along the 3-D surface crack front can be obtained from the elastic analysis. These values, along with the material gradient function, serve as inputs to the MBL model, which performs the simple 2-D elastic–plastic crack-tip analysis. Such approach is only possible with the development a new MBL model for FGMs—this represents the main scope of the present paper.

Many researchers have investigated the crack-tip stress fields in graded nonhomogeneous materials [6]. Delale and Erdogan [7] solved crack problems for nonhomogeneous materials assuming an exponential spatial variation of the elastic modulus. Eischen [8] adopted the eigenfunction technique to determine the leading terms of the asymptotic stress field in FGMs. Eischen observed that the asymptotic stress field near the crack-tip in a FGM is identical to that in a homogeneous material, i.e. the first two terms of the Williams’ solution. However, as the distance from the crack-tip increases, the higher-order terms become increasingly affected by the material gradient and the simple K – T dominance vanishes for FGMs. Studies have been performed to investigate the K – T dominance of graded nonhomogeneous materials. Gu and Asaro [9] studied crack deflection in FGMs where the crack plane is perpendicular to the material gradient direction. They showed that the size of the K – T dominant region decreases as the severity of the material nonhomogeneity increases. Marur and Tippur [10] also investigated the K – T dominance in FGMs. They argued that the homogeneous, asymptotic solution is not valid for FGMs and suggested that higher-order terms of the series must be considered to obtain good agreement between the analytical and numerical results. Recently, Anlas et al. [11] explored the extent and shape of the K – T dominant region in FGMs. They identified the relationship between the two different forms of asymptotic stress fields (i.e. the Williams [5] form and the modified Erdogan [12] form) and investigated the extent of validity of these fields.

In this study, we propose a new MBL framework for graded nonhomogeneous materials. The proposed model is based on a middle-crack tension, $M(T)$, specimen with traction boundary conditions applied to the top and lateral edges of the model. The crack plane lies parallel to the direction of the material gradation. We employ this model to analyze the elastic crack-tip fields of homogeneous and graded nonhomogeneous materials and compare the results with those obtained from the full-field calculations. Also, we investigate the K – T dominance of graded nonhomogeneous materials to determine the range of applicability of the proposed MBL model. Finally, we apply the proposed MBL model to predict the elastic–plastic crack-tip fields of a Ti/TiB FGM SE(T) specimen.

The remainder of the paper is organized as follows. Section 2 presents the concept of the new MBL model for graded nonhomogeneous materials and verifies the new MBL model. Section 3 describes the size effect of the MBL model via elastic crack-tip analysis and also describes the K – T dominance of graded nonhomogeneous materials. Section 4 presents an application of the MBL model to elastic–plastic crack-tip analysis of a Ti/TiB FGM SE(T) specimen. Finally, Section 5 provides some concluding remarks.

2. Modified boundary layer model for FGMs

For the MBL formulation of homogeneous materials, tractions or equivalent displacements (in general, displacements are preferred) are applied to the outer boundary of the disk-shaped finite element (FE) model based on the first two terms of the Williams’ solution. For mode I, the solution is given by [5]

$$\sigma_{ij}(r, \theta) = \frac{K_I}{\sqrt{2\pi r}} f_{ij}^I(\theta) + T \delta_{1i} \delta_{1j}, \quad \text{as } r \rightarrow 0, \quad (1)$$

where σ_{ij} denotes the stress tensor, K_I is the mode I stress intensity factor (SIF), T is the nonsingular stress parallel to the crack, and the angular function $f_{ij}^I(\theta)$ can be found in several references, e.g. [13,14]. In a plane-strain FE model, the equivalent boundary conditions can be applied in terms of displacements given as

$$\begin{aligned}
 u_1 &= \frac{K_I}{4\mu} \sqrt{\frac{r}{2\pi}} \left\{ (2\kappa - 1) \cos \frac{\theta}{2} - \cos \frac{3\theta}{2} \right\} + \frac{1 - \nu}{2\mu} Tr \cos \theta, \\
 u_2 &= \frac{K_I}{4\mu} \sqrt{\frac{r}{2\pi}} \left\{ (2\kappa + 1) \sin \frac{\theta}{2} - \sin \frac{3\theta}{2} \right\} - \frac{\nu}{2\mu} Tr \sin \theta,
 \end{aligned}
 \tag{2}$$

where μ is the shear modulus, κ is the bulk modulus, and ν is the Poisson’s ratio of the material.

For graded nonhomogeneous materials, the intrinsic length scale of the material must be introduced to the MBL framework. Simple application of the displacement boundary conditions, i.e. Eq. (2), on a nonhomogeneous model will not generate the corresponding K – T stress field—the displacement boundary conditions are functions of material properties but these have a gradient within the model. Thus, for graded nonhomogeneous materials, this new “degree of freedom” invalidates the use of the existing boundary layer framework most often used for homogeneous materials. A MBL model for graded nonhomogeneous materials must have the correct tractions or displacements to yield the desired K – T stress field. One approach applies tractions, Eq. (1), on the boundary of the disk-shaped model since the stress field is independent of the material properties. However, determination of the appropriate size of the disk-shaped model becomes a problem. The disk-shaped model must remain within the K – T dominant region, which depends on the material gradient, crack geometry, and loading conditions. Such problem involves two length scales, i.e. the fracture mechanics length scale and the intrinsic material length scale. These two length scales must be consistent within the model. In this sense, a MBL model for graded nonhomogeneous materials requires the convenience of applying tractions to the boundary and the consistency of the two length scales.

In this work, we select the middle-crack tension, M(T), specimen as the reference configuration for the new MBL model. Fig. 1 shows the geometry of this MBL model. The linear-elastic material is graded parallel to the crack plane and material properties are symmetric with respect to the centerline of the model. The symmetric loading conditions and material properties enable the use of a quarter model (shaded region in Fig. 1), tractions are easily applied to the top edge of the model and also to the lateral edge of the model. Now, the key task becomes the determination of the corresponding traction boundary conditions that generate the desired K – T field near the crack-tip. Fig. 2 shows the procedure to obtain the traction

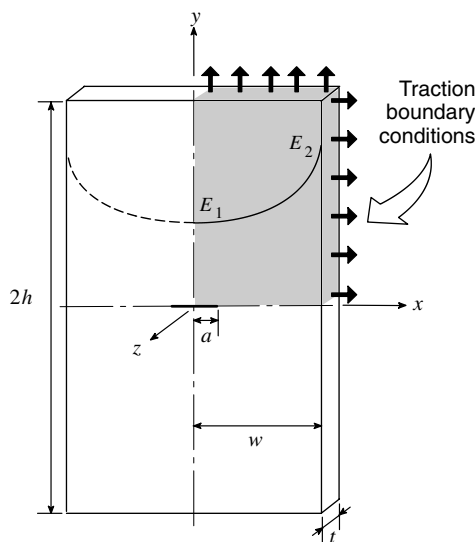


Fig. 1. Schematics of the proposed modified boundary layer model. Material properties are graded in the x -direction and symmetric with respect to the centerline of the model. The traction boundary conditions are applied to the top and lateral edges of the model.

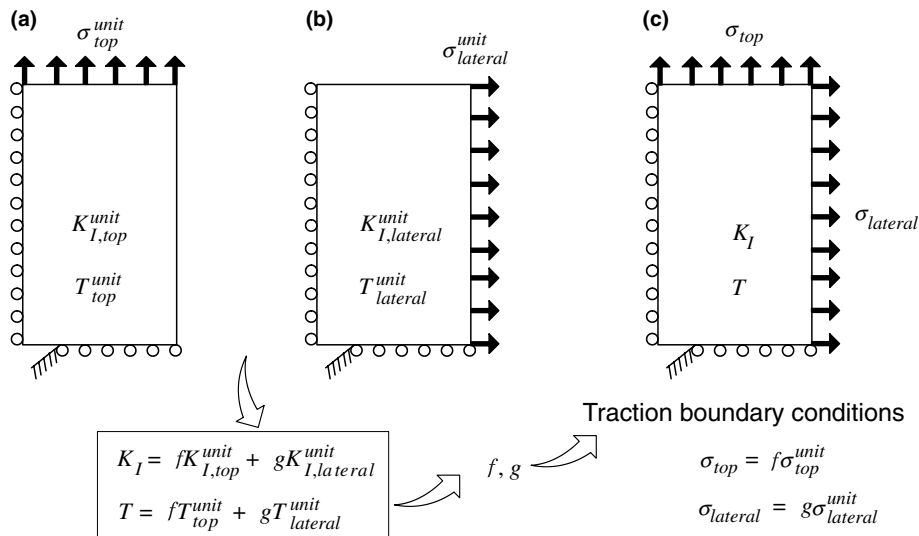


Fig. 2. Procedure to obtain the traction boundary conditions for the proposed modified boundary layer model. Unit traction applied to (a) the top edge and (b) the lateral edge of the model. Eqs. (3)–(5) yield the traction boundary conditions required to generate K_I and T at the crack-tip.

boundary conditions. First, a unit traction σ_{top}^{unit} is applied to the top edge of the model, Fig. 2(a). This unit traction produces $K_{I,top}^{unit}$ and T_{top}^{unit} at the crack-tip. As a second step, a unit traction $\sigma_{lateral}^{unit}$ is applied to lateral edge of the model, Fig. 2(b). Similarly, this unit traction produces $K_{I,lateral}^{unit}$ and $T_{lateral}^{unit}$ at the crack-tip. For homogeneous materials, $K_{I,lateral}^{unit} = 0$ since the stress parallel to the crack plane does not contribute to the mode I SIF. However, for graded nonhomogeneous materials, stress parallel to the crack plane contributes to the mode I SIF (through secondary bending as discussed in the following subsection). The SIF and T -stress values are proportional to the applied tractions. Let K_I and T denote the desired values of mode I SIF and the T -stress. Then these two values can be expressed by

$$K_I = fK_{I,top}^{unit} + gK_{I,lateral}^{unit}, \quad (3)$$

$$T = fT_{top}^{unit} + gT_{lateral}^{unit}, \quad (4)$$

where

$$f = \frac{\sigma_{top}}{\sigma_{top}^{unit}}, \quad g = \frac{\sigma_{lateral}}{\sigma_{lateral}^{unit}}, \quad (5)$$

where σ_{top} and $\sigma_{lateral}$ are the traction boundary conditions needed to obtain K_I and T . By using Eqs. (3)–(5), the traction boundary conditions for the MBL model can be easily determined for any desired K_I and T , Fig. 2(c). Two example problems (homogeneous and graded nonhomogeneous material) verify the proposed MBL model in the following subsection.

2.1. Verification of the proposed modified boundary layer model

Fig. 1 shows the geometries of the proposed MBL model, i.e. the M(T) specimen. For the following two examples, the crack half-length, a ; plate half-width, w ; plate half-height, h ; and plate thickness, t , are fixed such that $a/w = 0.1$, $h/w = 2$ and $t/w = 0.01$. Fig. 3 shows the 3-D FE mesh used in the present study. Symmetry conditions permit modelling of only one quarter of the specimen. The mesh consists of triquadratic (20-noded brick) elements with reduced ($2 \times 2 \times 2$) integration and has one-layer of elements through the thickness. All the nodes in the model are constrained in the thickness direction to obtain plane-strain conditions. Elements with quarter-point nodes and collapsed faces are used to model the crack-tip. The FE model has 37683 nodes and 5250 elements.

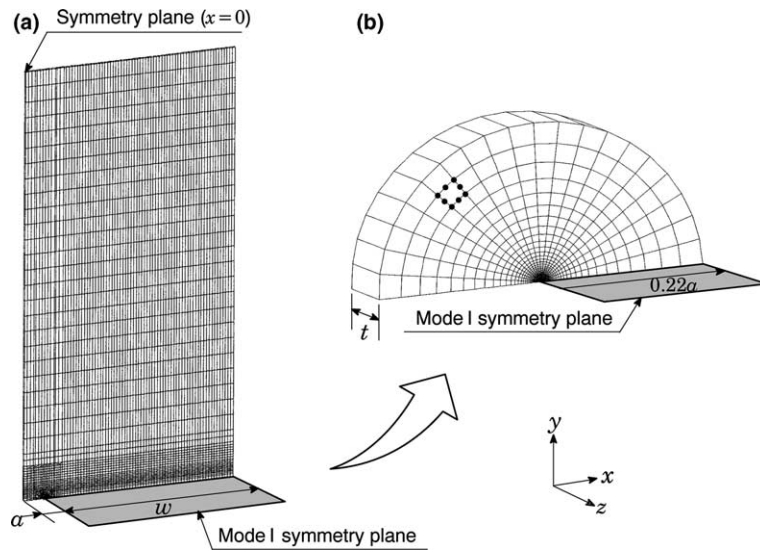


Fig. 3. Typical finite element mesh used in the present study: (a) overall view; (b) close-up view of the circular domain (67 rings) at the crack-tip.

The present study considers two sets of material properties, i.e. homogeneous and graded nonhomogeneous materials. For the homogeneous material, the Young's modulus $E(=E_1=E_2)$ is 1 (consistent units) and the Poisson's ratio ν is 0.3. For the graded nonhomogeneous material, ν is a constant ($=0.3$) and E is an exponential function:

$$E(x) = E_1 e^{\lambda x}, \quad (6)$$

where λ is the material nonhomogeneity parameter and $1/\lambda$ denotes the length scale of the material. In this example, E_1 and E_2 are 1 and 5 (consistent units), respectively. This corresponds to a material nonhomogeneity parameter $\lambda = 0.313$.

Conventional finite elements with constant material properties in each element, i.e. *homogeneous element*, have been used to analyze the behavior of graded materials with relatively fine meshes [15]. Recently, Kim and Paulino [16] presented a generalized isoparametric formulation (GIF) to calculate the elastic properties within an element. Jin et al. [17] further evaluated the plastic properties within an element using this approach. Such *graded elements* include the gradation effect at the element level and thus can substantially improve the solution quality based on the same mesh density, especially for higher-order graded elements [16]. Within graded elements, the calculation of stiffness, stress and other quantities requires the value of properties at integration points. With nodal values of material properties defined at each nodes, interpolation using element shape functions determines property values at integration points. The current study employs the nodal-value approach rather than the direct property sampling at the Gauss points [18].

Tractions applied to the top and lateral edges of the model are uniform for homogeneous materials. However, for graded nonhomogeneous materials, the uniform traction applied to the top edge of the model may not be equivalent to the far-field tension—due to the material gradient in the x -direction. Kim and Paulino [16] give the exact traction solution equivalent to the far-field tension for exponentially graded nonhomogeneous materials. If the height of the model (h) is sufficiently long, the uniform traction solution and the exact traction solution will generate the same result far away from the boundary (e.g. Saint Venant principle). In this study, for accuracy, the traction applied to the top edge of the model is determined from the solution given by Kim and Paulino [16].

2.1.1. Finite element analysis (FEA)

The numerical solutions are generated using WARP3D [19], a research code for nonlinear fracture mechanics. WARP3D employs an incremental-iterative, implicit formulation for analysis of fracture models

subjected to quasi-static and dynamic loading. Besides the conventional solid elements for homogeneous materials, this code also incorporates solid elements with graded elastic and plastic properties. Moreover, WARP3D incorporates the interaction integral technique to calculate SIFs and T -stresses in 3-D homogeneous [20–23] and functionally graded materials [24,25] (see Appendix A). The interaction integral method post-processes actual displacement, stress and strain fields of an equilibrium state for a boundary-value problem. Another selected equilibrium state supplies auxiliary fields that involve sought quantities such as stress intensity factors or T -stresses. A linear combination of actual fields with auxiliary fields described by Williams' solution [5], constitutes a third, superimposed, equilibrium state. The computation of J for this superimposed state leads to a conservation integral, composed of interacting actual and auxiliary terms, that permits direct calculation of stress intensity factors [20]. Alternative auxiliary fields enable the direct calculation of T -stresses [26].

In the present study, K_I and T -stress are calculated from the MBL model. These values are used to obtain the crack-tip stress field based on the Williams' solution (up to the second term). Also the crack-tip stress fields are directly obtained from the nodal stress values and these fields are compared with the Williams' solution.

2.1.2. Results: Homogeneous material

First, a unit traction ($\sigma_{\text{top}}^{\text{unit}} = 1$) is applied to the top edge of the model. This produces $K_{I,\text{top}}^{\text{unit}} = 1.25$ and $T_{\text{top}}^{\text{unit}} = -1$ (consistent units). The biaxiality ratio relates the T -stress to the stress intensity factor by

$$\beta = \frac{T\sqrt{\pi a}}{K_I}. \quad (7)$$

It is a well known fact that $\beta = -1$ for a homogeneous M(T) specimen with $a/w = 0.1$ [14]. This signifies that the ratio of the remote traction applied to the specimen to the T -stress at the crack-tip is -1 . Numerical results from the present study confirm that the T -stress is equal to a negative value of the unit traction. We now apply a unit traction ($\sigma_{\text{lateral}}^{\text{unit}} = 1$) to the lateral edge of the model. This produces $K_{I,\text{lateral}}^{\text{unit}} = 0$ and $T_{\text{lateral}}^{\text{unit}} = 1$. This result is obvious since the stress parallel to the crack plane is the T -stress and does not contribute to the mode I SIF.

Eqs. (3)–(5) determine the traction boundary conditions (σ_{top} and σ_{lateral}) required to obtain the desired K – T stress field. For example, if the desired values are $K_I = 5$ and $T = 0$, the traction boundary conditions are $\sigma_{\text{top}} = 4$ and $\sigma_{\text{lateral}} = 4$. Fig. 4(a) shows the normalized crack-tip stress field obtained from the MBL model with the traction boundary conditions simultaneously applied to the top ($\sigma_{\text{top}} = 4$) and the lateral ($\sigma_{\text{lateral}} = 4$) edges of the model. The normalized stress values ($\sigma_{ij}\sqrt{2\pi r}/K_I$) are plotted against the angle (θ/π) around the crack-tip. The normalized distance from the crack-tip (r/a) is 0.014. Fig. 4(a) also shows the stress field given by the Williams' solution, where $K_I = 5$ and $T = 0$. Two results show excellent agreement which demonstrate the applicability of the proposed MBL model to homogeneous materials.

2.1.3. Results: Nonhomogeneous material

The exact traction equivalent to the far-field unit traction (given by Kim and Paulino [16]) is applied to the top edge of the model. This produces $K_{I,\text{top}}^{\text{unit}} = 0.549$ and $T_{\text{top}}^{\text{unit}} = -0.477$. Since there is no material gradient in the y -direction, uniform unit traction, $\sigma_{\text{lateral}}^{\text{unit}} = 1$, is applied to the lateral edge of the model. This produces $K_{I,\text{lateral}}^{\text{unit}} = 0.292$ and $T_{\text{lateral}}^{\text{unit}} = 0.835$. Note the effect of $\sigma_{\text{lateral}}^{\text{unit}}$ to the mode I SIF. Also the T -stress is not equal to the applied unit traction as in the homogeneous case. This phenomenon is due to the material gradient and can be easily explained by observing the deformed shape and the stress distribution of the MBL model. Fig. 5 shows the stress distribution within the deformed FE model, where a unit traction is applied to the lateral edge. Fig. 5(a) shows the stress distribution in the y -direction (σ_{yy}). The top part of the model shows boundary effects (considering prescribed tractions at the top edge). However, this boundary effect does not affect the stress distribution at the symmetry plane ($y = 0$). Due to the secondary bending effect caused by the material gradient, the cracked region of the model suffers mode I loading. The deformed shape of the model shows the opening of the crack-face. Fig. 5(b) shows the stress distribution in the x -direction (σ_{xx}). Here again, the top part of the model shows boundary effects, which can be neglected. Also the stress above the crack is slightly lower than the applied traction (unit traction). Fig. 5 demonstrates that behaviors of graded nonhomogeneous

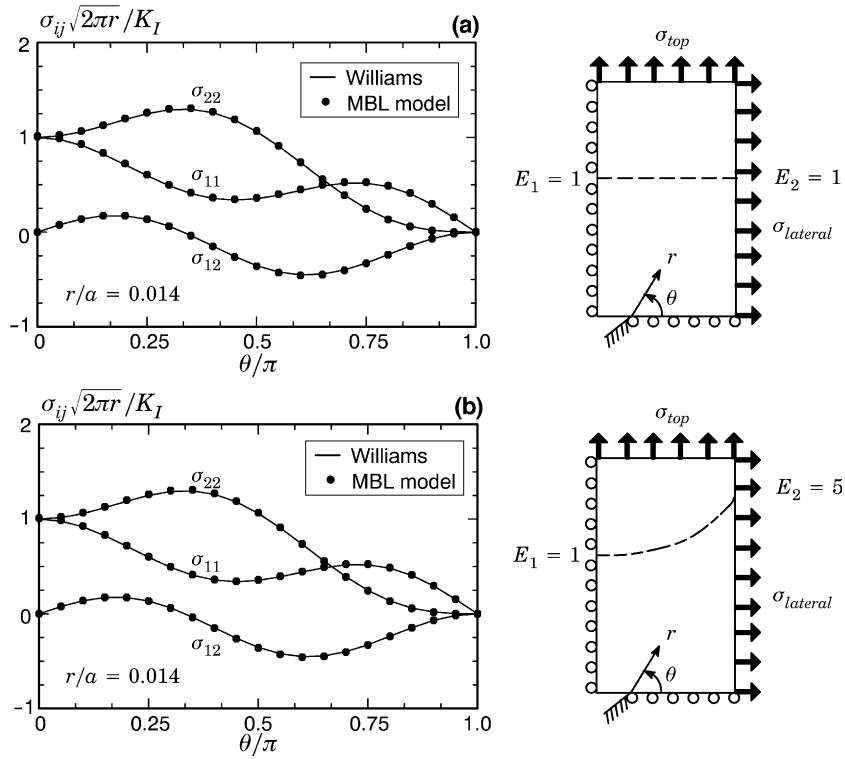


Fig. 4. Comparison of normalized stress values around the crack-tip obtained from Williams’ solution, Eq. (1), and proposed modified boundary layer (MBL) model: (a) homogeneous; (b) nonhomogeneous.

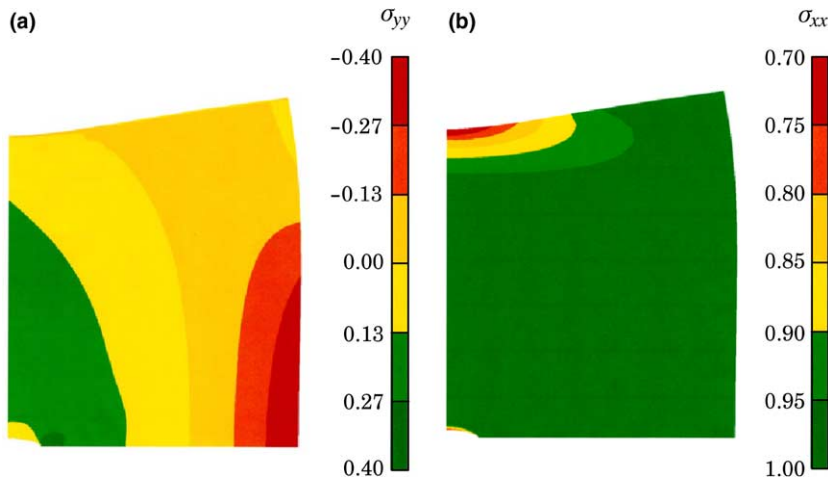


Fig. 5. Deformed shape and stress distribution of graded nonhomogeneous ($E_2/E_1 = 5$) FE model with unit traction applied to the lateral edge: stress distribution in (a) y -direction σ_{yy} ; (b) x -direction σ_{xx} .

materials are very much different from those of homogeneous materials. In this example, the Young’s modulus of the material increases exponentially in the x -direction; from 1 to 5. If the Young’s modulus of the material decreases in the x -direction; from 5 to 1, the secondary bending effect shown in Fig. 5(a) is in the opposite direction. This causes crack-closure and thus $K_{I,lateral}^{unit}$ is a negative value, which signifies that the traction applied to the lateral edge reduces the total K_I .

Nevertheless, the traction boundary conditions (σ_{top} and σ_{lateral}) can still be determined from Eqs. (3)–(5). For example, if the desired values are $K_I = 5$ and $T = 0$, the traction boundary conditions are $\sigma_{\text{top}} = 7$ and $\sigma_{\text{lateral}} = 4$. Fig. 4(b) shows the normalized crack-tip stress field obtained from the MBL model, where $\sigma_{\text{top}} = 7$ and $\sigma_{\text{lateral}} = 4$. The normalized distance from the crack-tip (r/a) is 0.014. Fig. 4(b) also shows the stress field given by the Williams' solution, where $K_I = 5$ and $T = 0$. Two results show excellent agreement which verifies the applicability of the proposed MBL model to graded nonhomogeneous materials. Fig. 4(b) also confirms the fact that the asymptotic stress field very close to the crack-tip in a graded nonhomogeneous material is exactly same as the singular term of the Williams' solution [7,8].

2.2. Remarks on the proposed modified boundary layer model

Two example problems described in the previous subsection show that the proposed MBL formulation is applicable to homogeneous and nonhomogeneous (exponentially graded) materials. Since the traction boundary conditions compensate for the material gradient, this formulation can be employed to any type of material gradient (e.g. constant, linear, exponential) in the x -direction—different material gradient yields different traction boundary conditions for the same desired K_I and T . Furthermore, the crack geometry of the proposed MBL model does not have to be fixed to $a/w = 0.1$.

The “standard” MBL formulation, i.e. the disk-shaped model most often used for homogeneous materials, does not involve an explicit crack or ligament length. A dimensional scale is introduced by the radius at which displacements are applied. However, the MBL model proposed in the present work is based on a M(T) specimen, which is a boundary-valued model. Therefore, the MBL model has its own K – T dominant region. This introduces a size effect, i.e. the size of the K – T dominant region of the MBL model depends on the size of the model itself. Another issue related to this problem is the extent of applicability of the K – T stress field for graded nonhomogeneous materials. Since the MBL model can only provide the K – T stress field, dominance of this field must be investigated for different cracked geometries and material gradients. These aspects are investigated in the following section.

3. Elastic crack-tip analysis and K – T dominance of FGMs

In this section, we investigate two problems. First, we investigate the size effect of the proposed MBL model. This work attempts to determine the appropriate size of the model which can fully describe the K – T stress field of a full cracked structure (or specimen). Then, we investigate the dominance of the K – T field in elastic, graded nonhomogeneous materials. This is achieved by comparing the actual crack-tip stress field with the K – T stress field. This study provides insight into the effect of material gradient and crack geometry to the K – T dominance of FGMs.

3.1. Size effect of the proposed modified boundary layer model

In the present study, single-edged tension, SE(T), specimen is considered as the full cracked structure. SE(T) specimen with a short crack is a good representation of a 3-D surface crack in a plate under mode I loading. Since our ultimate objective is to apply the MBL model to 3-D surface crack problems, SE(T) specimen serves as an appropriate example. Fig. 6 shows the geometry of the SE(T) specimen considered in the present study. Symmetry conditions permit modelling of only half of the specimen. For the following examples, the crack length, $a = 2$; plate width, $w = 20$; plate half-height, $h = 60$; and plate thickness, $t = 0.2$ (consistent units), which yield $a/w = 0.1$, $h/w = 3$, $t/w = 0.01$.

The three-dimensional FE mesh for the SE(T) specimen is similar to the mesh employed for the proposed MBL model. The mesh consists of triquadratic (20-noded brick) elements with reduced ($2 \times 2 \times 2$) integration and has one-layer of elements through the thickness. All the nodes in the model are constrained in the thickness direction to obtain plane-strain conditions. Elements with quarter-point nodes and collapsed faces are used for modelling the crack-tip. The FE model has 37683 nodes and 5250 elements. Homogeneous and nonhomogeneous material properties are considered. For homogeneous material, the Young's modulus is a unit value, i.e. $E_1 = E_2 = 1$ (consistent units). For nonhomogeneous material, the Young's modulus varies

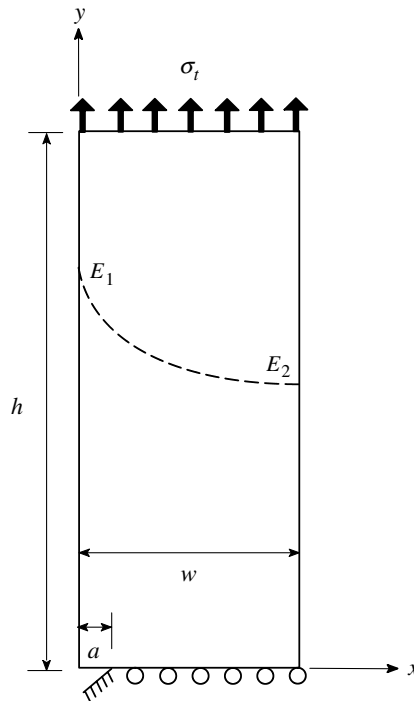


Fig. 6. SE(T) specimen with material properties graded in the x -direction.

exponentially according to $E(x) = E_1 e^{\lambda x}$. In this example, $E_1 = 5$ and $E_2 = 1$ which corresponds to $\lambda = -0.08$. Poisson's ratio is a constant, $\nu = 0.3$, for both cases. The tensile stress, σ_t , is applied to the top edge of the model. The tensile stress is a uniform value for the homogeneous material. For the exponentially graded non-homogeneous material, the tensile stress follows the solution given by Kim and Paulino [16]. WARP3D is used to perform the linear-elastic FE analysis. Elastic crack-tip stress field is obtained from the nodal stress values. Interaction integral technique implemented in WARP3D calculates the K_I and T -stress. These values are used to calculate the K - T stress field (Williams' solution) using Eq. (1). These values also serve as the desired K_I and T , Eq. (3), for the proposed MBL model.

As mentioned in the previous section, the proposed MBL model is a boundary-value model and thus has a K - T dominant region, which changes in size with the model size. In order to fully describe the K - T stress field of the full cracked structure, the K - T dominant region of the MBL model must be larger than that of the full cracked structure, i.e. the SE(T) specimen. In the present study, two different sized MBL models are employed to investigate the size effect of the proposed MBL model. The first model, "model A", has a crack length equal to the SE(T) specimen and the second model, "model B", has a crack length eight times the SE(T) crack length. For both models $a/w = 0.44$. Homogeneous and graded nonhomogeneous materials are considered. Since the stress in the y -direction, σ_{yy} , is the dominant stress, the following results only compare σ_{yy} .

3.1.1. Homogeneous material

Fig. 7 shows the plot of normalized opening stress, σ_{yy}/σ_t , at the symmetry plane ($\theta = 0$) versus the normalized distance from the crack-tip, $r/a_{SE(T)}$. The opening stress is normalized by the tensile stress applied to the SE(T) specimen and the distance from the crack-tip is normalized by the crack length of the SE(T) specimen. Fig. 7 shows the actual stress field obtained from the FE analysis of the SE(T) specimen, stress field based on the Williams' asymptotic solution, and the stress field obtained from the two MBL models. All solutions show good agreement near the crack-tip, i.e. $r \rightarrow 0$. The actual stress field deviates from the Williams' asymptotic solution as the distance from the crack-tip increases. This is due to the effect of the higher-order terms of the Williams' solution. Difference between these two results determines the K - T dominance, which will be discussed in the following subsection. Here, we focus on the size effect of the MBL model. Results obtained

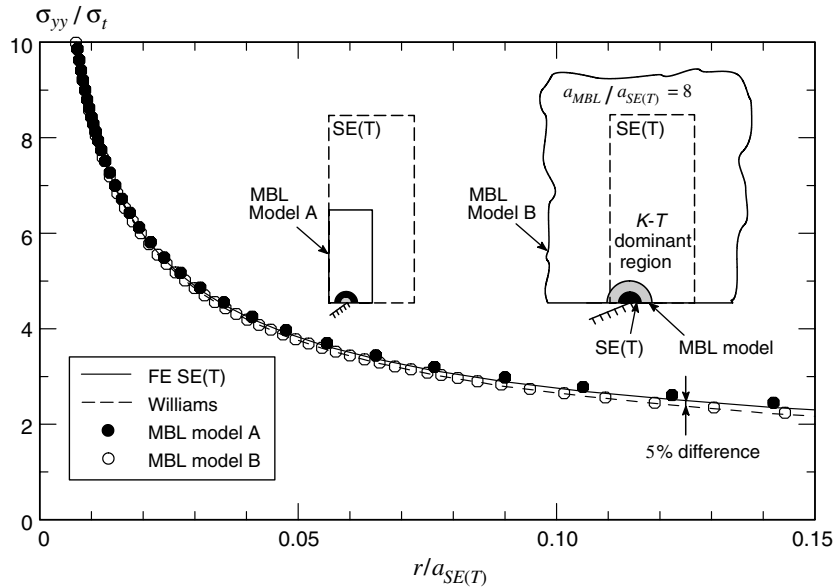


Fig. 7. Comparison of normalized opening stress at symmetry plane ($\theta = 0$) obtained from FE analysis, Williams' asymptotic solution, and two proposed modified boundary layer (MBL) models. Homogeneous material.

from the two MBL models, i.e. “model A” and “model B”, demonstrate the size effect of the MBL model. The stress field of “model A”, which has the same crack length as the SE(T) specimen, deviates from the Williams' asymptotic solution as the distance from the crack-tip increases. The illustration in Fig. 7 depicts that the $K-T$ dominant region of “model A” is within the $K-T$ dominant region of the SE(T) specimen. The stress field of “model A” starts to deviate from the Williams' asymptotic solution at the distance where the $K-T$ dominance vanishes for the MBL model. On the other hand, for “model B”, which has a crack length eight times larger than that of the SE(T) specimen, the $K-T$ dominant region of the SE(T) specimen is contained within that of the MBL model. Under these conditions, the stress field obtained from “model B” fully explains the $K-T$ dominant region of the SE(T) specimen. Fig. 7 shows that the stress field of “model B” matches the Williams' asymptotic solution up to $r/a_{SE(T)} = 0.15$.

3.1.2. Nonhomogeneous material

The size of the MBL model does not affect the material properties for homogeneous materials. However, for graded nonhomogeneous materials, the size of the proposed MBL model affects the material gradation. For any model size, the material nonhomogeneity parameter (λ) and the material property (Young's modulus) at the crack-tip must be equal to those of the full cracked structure. In this example, the Young's modulus of the SE(T) specimen is exponentially graded from $E_1 = 5$ to $E_2 = 1$ and the material nonhomogeneity parameter $\lambda = -0.08$. The Young's modulus at the crack-tip $E_{tip} = 4.26$. Based on these values, gradation of the Young's modulus within the MBL model is determined by

$$\begin{aligned} E_1 &= E_{tip}e^{-\lambda a}, \\ E_2 &= E_{tip}e^{\lambda(w-a)}, \end{aligned} \tag{8}$$

where a is the crack length and w is the half-plate width of the MBL model. E_1 and E_2 are the Young's modulus at the center and lateral edge of the model, respectively (Fig. 8). In this study, we employ “model B” as the MBL model. Illustration in Fig. 8, depicts the material gradient of the MBL model. The Young's modulus of the MBL model is graded from $E_1 = 15.32$ to $E_2 = 0.84$. Fig. 8 shows the plot of normalized stress, σ_{yy}/σ_t , at the symmetry plane ($\theta = 0$) versus the normalized distance from the crack-tip, $r/a_{SE(T)}$, for graded nonhomogeneous material. Fig. 8 shows the actual stress field obtained from the FE analysis of the SE(T) specimen, stress field based on the Williams' asymptotic solution, and the stress field obtained from the MBL model

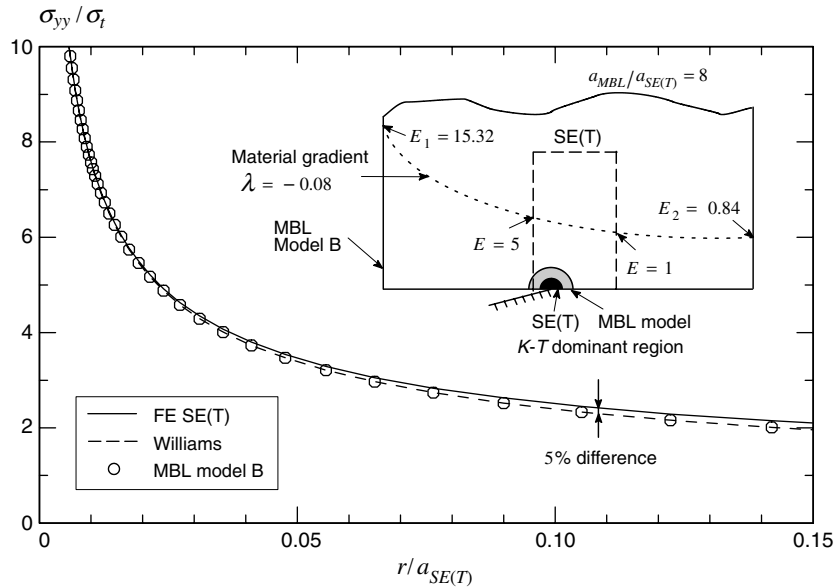


Fig. 8. Comparison of normalized opening stress at symmetry plane ($\theta = 0$) obtained from FE analysis, Williams' asymptotic solution, and proposed modified boundary layer (MBL) model (Model B). The Young's modulus is exponentially graded in the modified boundary layer model.

("model B"). Results are very similar to those of the homogeneous example where all solutions agree well very near the crack-tip. Fig. 8 also demonstrates that the proposed MBL model can fully explain the K - T dominant region of a graded nonhomogeneous material, provided that it has a larger K - T dominant region compared to that of a full cracked structure.

As described above, the material gradient of the MBL model can be determined from Eq. (8). However, if the full cracked structure, i.e. SE(T) specimen, has a relatively severe material gradient, the values of the material property (Young's modulus) would be extremely large or very close to zero either at the center or the lateral edge of the MBL model. In the present study, another method is adopted to assign the material gradient to the MBL model. As illustrated in Fig. 9, the material property of the MBL model is graded only in the region corresponding to the SE(T) specimen. The other regions of the MBL model have homogeneous material properties, i.e. $E_1 = 5$ and $E_2 = 1$. Fig. 9 shows the actual stress field obtained from the FE analysis of the SE(T) specimen, stress field based on the Williams' asymptotic solution, and the stress field obtained from the MBL model with material property graded only in the region corresponding to the SE(T) specimen. Results are exactly same as the results shown in Fig. 8. Application of this method to elastic-plastic analysis is presented in Section 4.

3.2. K - T dominance of graded nonhomogeneous materials

The MBL model generates the K - T stress fields for homogeneous and graded nonhomogeneous materials for a desired values of K_I and T . Now the question becomes how far away from the crack-tip does the K - T field match with the actual stress field. In this study, we compare the actual stress field with the K - T stress field and investigate the extent of the K - T dominance for SE(T) specimen (homogeneous and nonhomogeneous materials). We define the K - T dominant region by comparing the normalized opening stress, σ_{yy}/σ_t , at the symmetry plane. The K - T dominant region is defined as the region where the actual and asymptotic stresses differ within 5%. For example, Fig. 7 shows the actual stress field and the asymptotic stress field for a homogeneous SE(T) specimen ($a/w = 0.1$). Two results show a 5% difference at $r/a_{SE(T)} = 0.124$, i.e. the distance from the crack-tip is 12.4% of the SE(T) specimen crack length. Fig. 8 shows the crack-tip stress field for a graded nonhomogeneous SE(T) specimen ($E_2/E_1 = 5$, $a/w = 0.1$). The actual stress field and the asymptotic

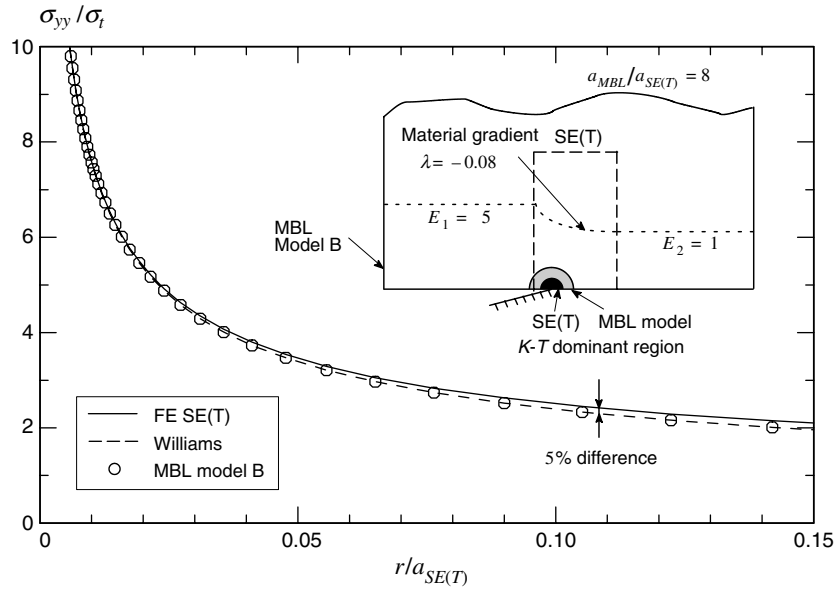


Fig. 9. Comparison of normalized opening stress at symmetry plane ($\theta = 0$) obtained from FE analysis, Williams' asymptotic solution, and proposed modified boundary layer (MBL) model (Model B). Young's modulus is exponentially graded only in the region corresponding to the SE(T) specimen.

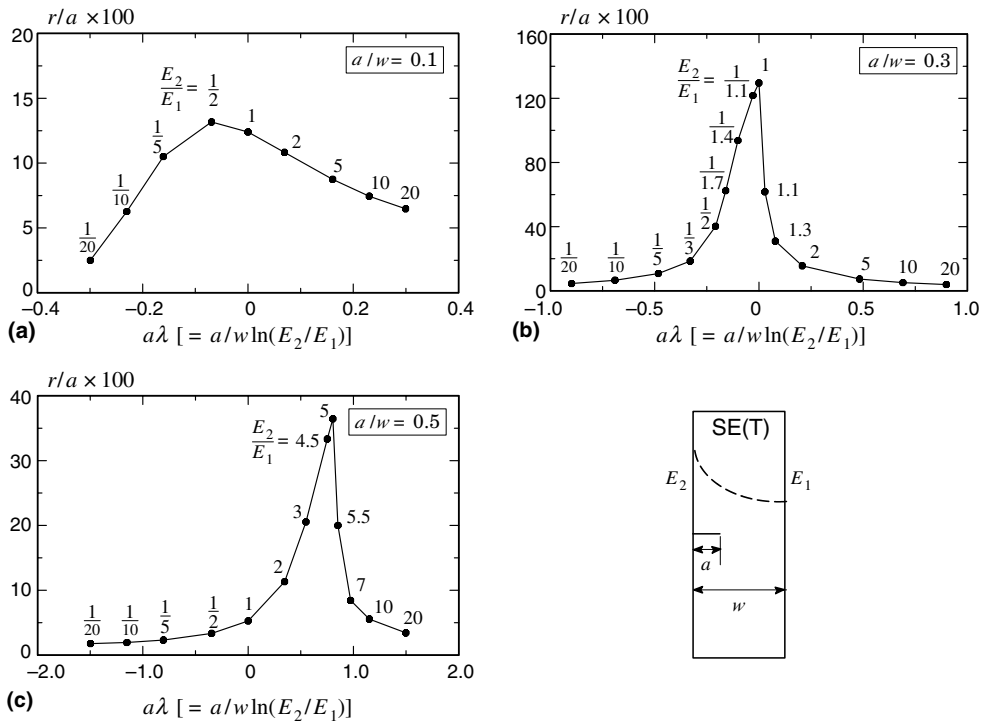


Fig. 10. Extent of the K - T dominance for SE(T) specimen considering various material gradients and geometrical configurations.

solution show a 5% difference at $r/a_{SE(T)} = 0.108$. Due to the material gradient, the K - T dominant region slightly reduces in size compared to that of the homogeneous material.

We further investigate the K – T dominance of graded nonhomogeneous materials considering various material gradients and crack geometries. Material gradients range from $E_2/E_1 = 1/20$ to $E_2/E_1 = 20$. The geometry considered in the present study is a SE(T) specimen with three different crack lengths, i.e. $a/w = 0.1, 0.3, 0.5$. Fig. 10 shows the extent of the K – T dominance for various material gradients and geometries considered in the present study. The extent of the K – T dominance ($r/a \times 100$) is plotted against the normalized material nonhomogeneity parameter, $a\lambda = a/w \ln(E_2/E_1)$, which represents the material gradient. The maximum extent of the K – T dominance is obtained at different material gradients for each geometry. For $a/w = 0.3$, the homogeneous material ($E_2/E_1 = 1$) shows the maximum extent of K – T dominance. For $a/w = 0.5$, the maximum extent of the K – T dominance is obtained at $E_2/E_1 = 5$. Results shown in Fig. 10 demonstrate that the maximum range of K – T dominance does not always prevail for homogeneous materials. For a certain range of material gradient for $a/w = 0.5$, the size of the K – T dominant region increases as the material nonhomogeneity increases. Fig. 10 also shows that the extent of the K – T dominance is less than $r/a \times 100 = 15$ for most of the material gradients and geometries considered in the present study. Fig. 10 also shows the valid extent of the MBL model for each material gradient and crack geometry. The crack-tip stress field of the MBL model can match (within 5%) that of the SE(T) specimen within the ranges shown in Fig. 10. Moreover, to obtain small scale yielding conditions in nonlinear analysis, the fracture process zone (e.g. plastic zone) must remain well within the K – T dominant region. It will be shown in the following section that it is valid to employ the proposed MBL model if the size of the region affected by the fracture process zone is approximately half the size of the K – T dominant region.

4. Application to elastic–plastic crack-tip analysis

This section describes the application of the proposed MBL model to elastic–plastic (nonlinear) crack-tip analysis. We employ the MBL model to analyze the elastic–plastic crack-tip field of a Ti/TiB FGM [27] SE(T) specimen.

4.1. Ti/TiB FGM SE(T) specimen

The company CERCOM Inc. developed the Ti/TiB FGM/LB (functionally graded material/large bulk) system in a layered structural form for potential armor applications [28]. In this study, we consider a Ti/TiB FGM SE(T) specimen with a continuously graded elastic–plastic material properties. Fig. 11 depicts the geometry and the material property variation of the Ti/TiB FGM SE(T) specimen. The idealized FGM composition varies from 100% TiB (ceramic) at the cracked surface to 100% Ti (metal) at the uncracked surface—the actual material variation from processing is presented in Ref. [27]. Thus ideally, the volume fraction

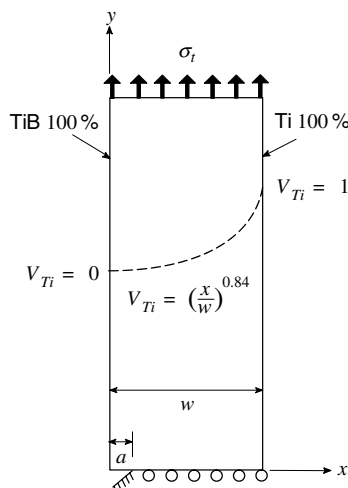


Fig. 11. Idealization of Ti/TiB FGM SE(T) specimen. The material gradient is expressed in terms of the volume fraction of Ti.

Table 1
Material properties of Ti and TiB

Materials	Young's modulus (GPa)	Poisson's ratio	Yield stress (MPa)	Hardening exponent	Critical J -integral (J_{IC}) (kJ/m ²)
Ti	107	0.34	450	14	24 ^a
TiB	375	0.14	–	–	0.11

^a Estimated from the experimental crack initiation load [17].

of Ti (V_{Ti}) varies from zero at the cracked surface to one at the uncracked surface. Table 1 lists the material properties of Ti and TiB (data from Refs. [17,29,30]). The volume fraction of Ti within the specimen is expressed as a simple power function, $V_{Ti} = (x/w)^p$, where the power exponent $p = 0.84$ [17].

While the classical Hooke's law describes the linear-elastic response of FGMs with the elastic properties approximately evaluated by simplified micromechanics models [31] (for conventional composite), determination of the elastic–plastic behavior of FGMs remains as a challenging task. Previous studies [17,29,32,33] have adopted the J_2 flow theory for ceramic/metal FGMs and evaluated the material properties using the volume fraction based model proposed by Tamura et al. [34] (so called TTO model). The present study also employs this engineering method to estimate the elastic–plastic behavior of the Ti/TiB FGM. The TTO model relates the uniaxial stress and strain of a two-phase composite to the corresponding average uniaxial stresses and strains of the two constituent materials (see Appendix B for details). The material-dependent parameter q should be calibrated to match the measured flow properties of tensile specimen extracted from monolithic composites of the FGM constituents. Because such data remains unavailable for the Ti/TiB FGM, we adopt $q = 4.5$ GPa as in previous studies [17,29,32,33]. Fig. 12 shows the elastic–plastic material properties (Young's modulus E , Poisson's ratio ν , yield stress σ_{YS} , and the power-law hardening exponent n) of the Ti/TiB FGM SE(T) specimen obtained from the TTO model.

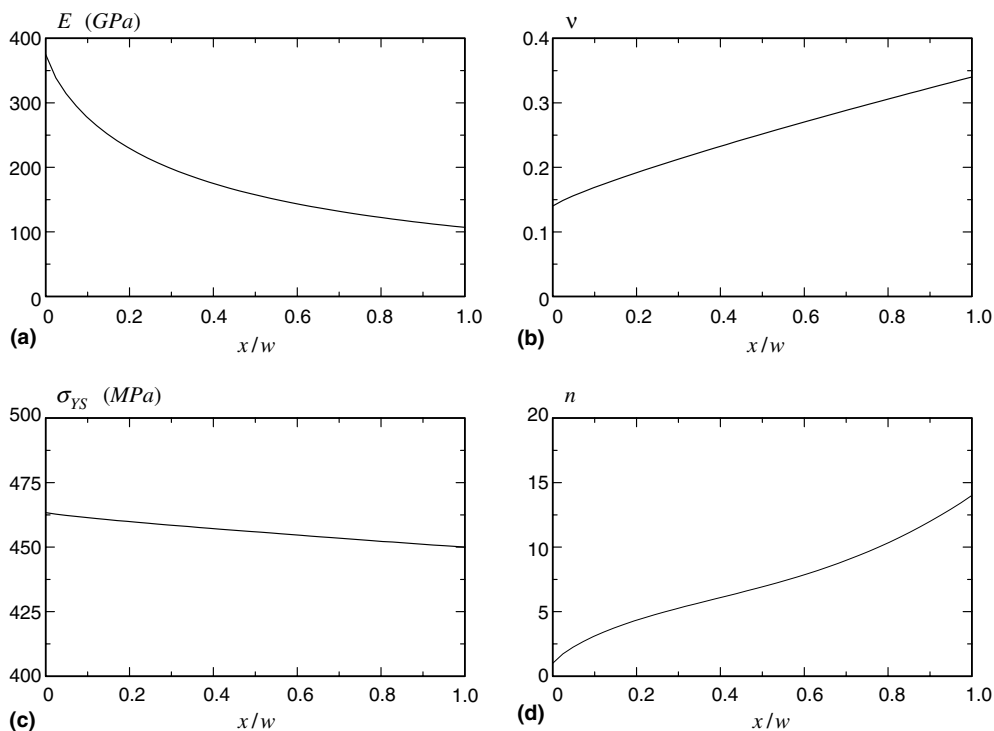


Fig. 12. Material properties of Ti/TiB FGM SE(T) specimen obtained from the TTO model.

The present study considers two Ti/TiB FGM SE(T) specimens ($w = 20\text{mm}$) with different crack length, i.e. $a = 2$ and 8.8mm , which yield $a/w = 0.1$ and 0.44 , respectively. For $a/w = 0.1$, the crack-tip is located at a position where the volume fraction of Ti is 14% ($V_{Ti} = 0.14$). The volume fraction of Ti at the crack-tip is 50% ($V_{Ti} = 0.5$) for $a/w = 0.44$. Thus, for both cases, the crack-tip is located within a relatively brittle region of the FGM system. Table 2 lists the material properties at the crack-tip for the two cases considered.

4.2. Elastic–plastic crack-tip analysis

Fig. 13 depicts the set-up of the MBL model for elastic and elastic–plastic analysis. Here, we employ “model B” from the previous section as the MBL model. The material gradient of the MBL model is expressed in terms of volume fraction of Ti. Since the volume fraction of Ti must be between zero and one, the material properties are graded only in the region corresponding to the SE(T) specimen. The other regions of the MBL model have either homogeneous material properties of Ti ($V_{Ti} = 1$) or TiB ($V_{Ti} = 0$) as shown in Fig. 13.

Fig. 14 illustrates the procedure adopted in the present study to perform elastic–plastic analysis. First, we perform elastic analysis for the SE(T) specimen, considering only the elastic material properties (E and ν). The tensile stress (σ_t) is applied to the SE(T) specimen to obtain a K_I value slightly (3%) less than the fracture toughness (K_{IC}) at the crack-tip, which is estimated from Ref. [17]. The elastic analysis yields K_I and T , which are used to determine the traction boundary conditions for the MBL model. The traction boundary conditions are determined from the elastic analysis of the MBL model only considering E and ν (see Fig. 2). The determined traction boundary conditions are applied to the MBL model for elastic–plastic analysis. The elastic and plastic material properties (E , ν , σ_{YS} , and n) are considered in the elastic–plastic analysis of the MBL model. The crack-tip stress and strain field and the plastic zone size and shape are analyzed in the elastic–plastic analysis. These results are compared with those obtained from the elastic–plastic analysis of the SE(T) specimen to validate the applicability of the MBL model to elastic–plastic crack-tip analysis.

Table 2
Crack-tip material properties obtained from the TTO [34] model for the Ti/TiB FGM SE(T) specimens consider in the present study

a/w	$V_{Ti,tip}$	E_{tip} (GPa)	ν_{tip}	$\sigma_{YS,tip}$ (MPa)	n_{tip}
0.1	0.14	279	0.17	461	3.1
0.44	0.5	167	0.24	457	6.4

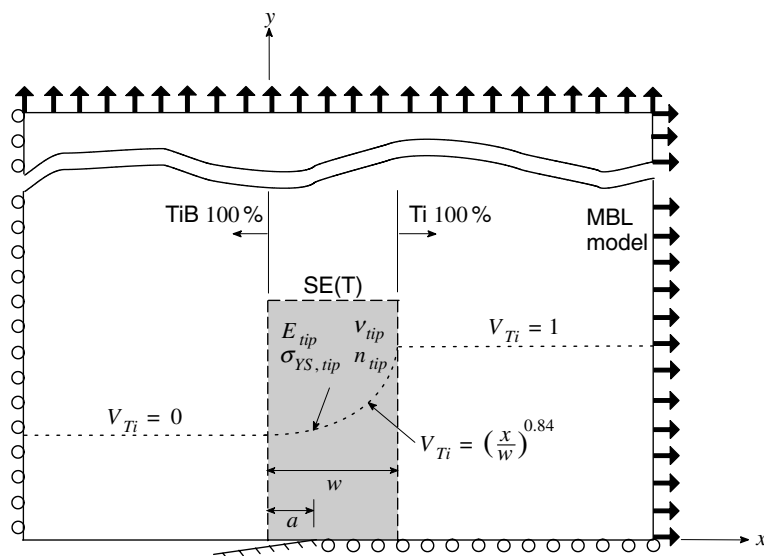


Fig. 13. Set-up of modified boundary layer (MBL) model for Ti/TiB FGM. Material properties are graded only in the region corresponding to the SE(T) specimen.

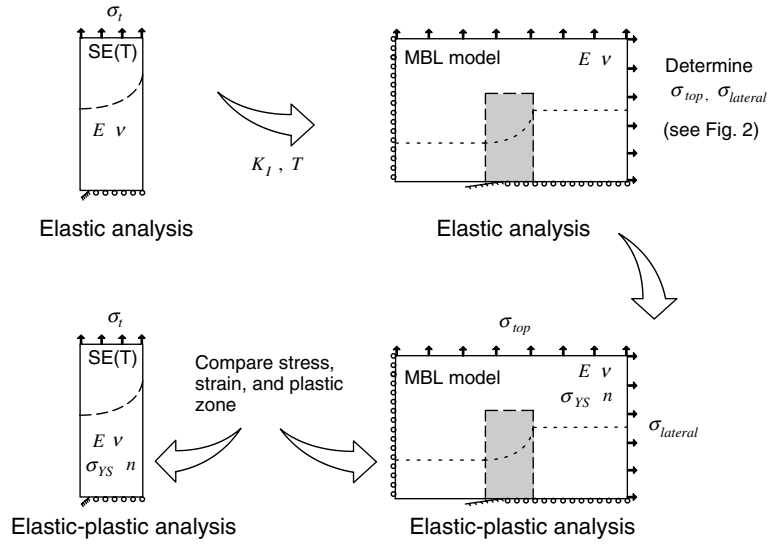


Fig. 14. Procedure adopted to verify the application of the proposed modified boundary layer (MBL) model to elastic-plastic (nonlinear) crack-tip analysis.

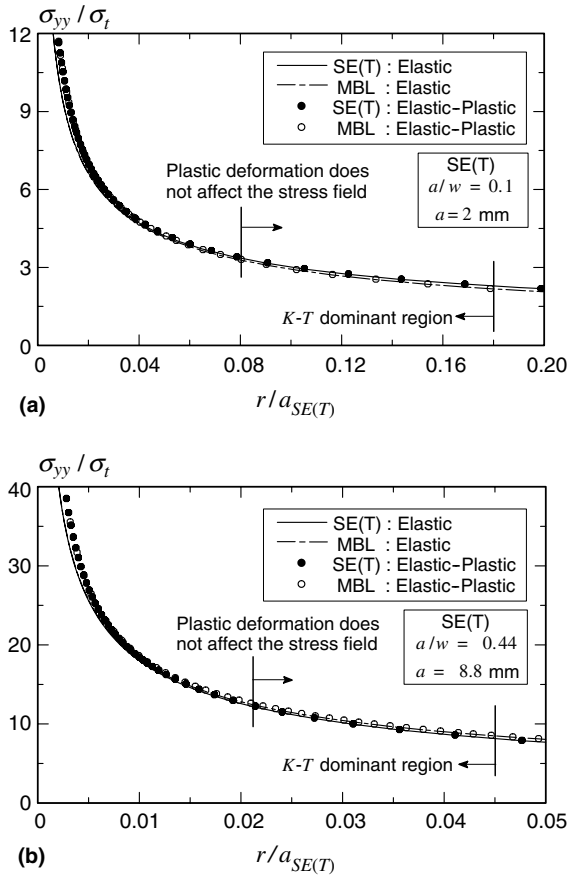


Fig. 15. Comparison of normalized opening stress at symmetry plane ($\theta = 0$) obtained from the elastic and elastic-plastic analyses of proposed modified boundary layer (MBL) model considering SE(T) specimen.

The FE meshes used for elastic–plastic analyses are similar to those used for elastic analyses. The mesh consists of triquadratic (20-noded brick) graded elements with reduced ($2 \times 2 \times 2$) integration. All the nodes in the model are constrained in the thickness direction to obtain plane strain conditions. However, for elastic–plastic analysis, the crack-tip elements have half-point nodes and crack-tip constraints permit blunting deformations. Deformation plasticity and small-strain formulation are employed for the elastic–plastic analysis.

4.3. Elastic and elastic–plastic analysis results

The elastic and elastic–plastic analysis results obtained from the two Ti/TiB SE(T) specimens ($a/w = 0.1$ and 0.44) and the MBL models are shown in Fig. 15. The normalized opening stress, σ_{yy}/σ_t , at the symmetry plane ($\theta = 0$) is plotted against the normalized distance from the crack-tip, $r/a_{SE(T)}$. The extent of the K – T dominant region is determined by comparing the elastic analysis results obtained from the SE(T) specimen and the MBL model. The elastic–plastic analysis results of the SE(T) specimen and the MBL model show excellent agreement near the crack-tip but show a difference as the distance from the crack-tip increases. Comparison between elastic and elastic–plastic analysis results (for both the SE(T) specimen and the MBL model) shows the effect of the plastic deformation to the crack-tip stress field. However, as the distance from the crack-tip increases, the two stress fields become identical. The region affected by the plastic deformation is approximately half the size of the K – T dominant region. This confirms that SSY conditions are satisfied and thus validates the applicability of the proposed MBL model. Results shown in Fig. 15 also demonstrate that the material properties assigned to the MBL model, i.e. material graded only in the region corresponding to the SE(T) specimen (Fig. 13), are valid for elastic and elastic–plastic analysis for the geometries and material properties considered.

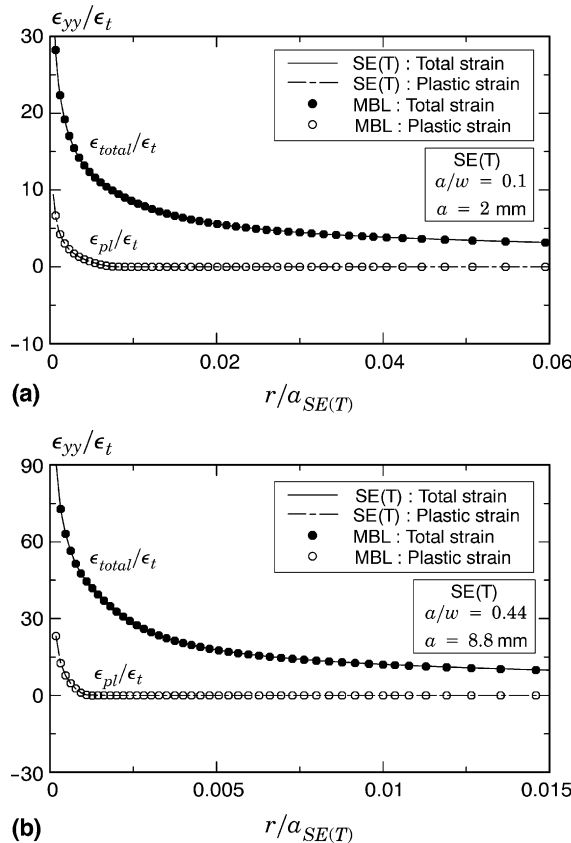


Fig. 16. Comparison of normalized opening total strain (ϵ_{total}) and plastic strain (ϵ_{pl}) at symmetry plane ($\theta = 0$) obtained from the elastic–plastic analysis of proposed modified boundary layer (MBL) model considering SE(T) specimen.

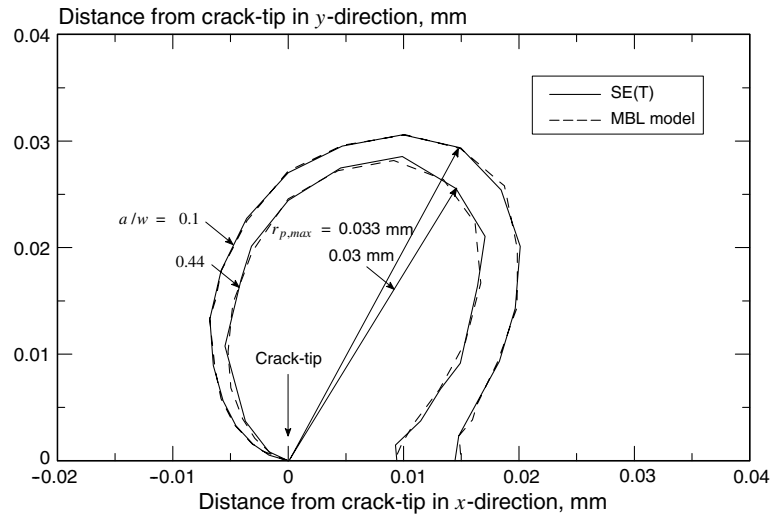


Fig. 17. Plastic zone size and shape of Ti/TiB FGM SE(T) specimen.

Fig. 16 shows the plot of normalized opening strain, ϵ_{yy}/ϵ_t , at the symmetry plane ($\theta = 0$) versus the normalized distance from the crack-tip, $r/a_{SE(T)}$, obtained from the two Ti/TiB SE(T) specimens ($a/w = 0.1$ and 0.44). The total strain, ϵ_{total} , and the plastic strain, ϵ_{pl} , is normalized by ϵ_t , which is defined as σ_t/E_{tip} . The plastic strain is calculated according to

$$\epsilon_{pl} = \epsilon_{total} - \frac{1}{E_{tip}} \{ \sigma_{yy} - \nu_{tip} (\sigma_{zz} + \sigma_{xx}) \}. \quad (9)$$

Results obtained from the MBL model show excellent agreement with those obtained from the SE(T) specimen. The plastic strain fields in Fig. 16 show the size of the plastic zone at the symmetry plane. Fig. 17 shows the size and shape of the plastic zone obtained from the proposed MBL model and the SE(T) specimen. Boundaries of the plastic zone are obtained from a stress contour, where the von Mises stress equals the yield stress at the crack-tip. The maximum plastic zone size, $r_{p,max}$, is defined as the distance measured from the crack-tip to the furthest point on the boundary of the plastic zone. The maximum size and shape of the plastic zone obtained from the MBL model and the SE(T) specimen match well for both cases ($a/w = 0.1$ and 0.44). Results shown in Figs. 15–17 validate the applicability of the MBL model to elastic–plastic crack-tip analysis.

5. Concluding remarks

This paper describes the development of a new MBL model for graded nonhomogeneous materials (e.g. FGMs) under mode I, plane-strain conditions where the crack plane is parallel to the material gradient. The proposed MBL model is based on a M(T) specimen with traction boundary conditions applied to the top and lateral edges of the model. For linear behavior, a simple superposition method determines the traction boundary conditions. These traction boundary conditions compensate for the material gradient and thus enable the application of the MBL model to various material gradients. Moreover, the two length scales, i.e. the fracture mechanics length scale and the intrinsic material length scale, are consistent within the model. The elastic crack-tip stress fields obtained from the proposed MBL model show excellent agreement with those obtained from the classical Williams' solution (up to two terms). For evaluating the crack-tip field of a cracked structure, i.e. the SE(T) specimen in the present study, the size of the MBL model must be determined so that the K – T dominant region of the SE(T) specimen is embedded within that of the MBL model.

A parametric study provides the extent of the K – T dominance for graded nonhomogeneous SE(T) specimens. The present results, while not exhaustive, provide insights into the K – T dominance of graded nonhomogeneous materials considering material gradient and crack geometry. These results also serve as a guideline for

applying the MBL model to FGMs. Elastic–plastic crack-tip analysis results show that the MBL model is applicable even when the size of the region affected by the fracture process zone is approximately half the size of the K – T dominant reign. Application to Ti/TiB FGM SE(T) specimen demonstrates the usefulness of the proposed MBL model to elastic–plastic analysis of cracks in FGM configurations.

Various elastic–plastic fracture mechanics problems, which utilizes the standard MBL model for homogeneous materials (e.g. effect of T -stress on plastic zone size and shape, constraint effects, crack growth analysis, etc.), can now be solved for FGMs by using the proposed MBL model. Investigation of crack growth (parallel to the material gradient) in FGMs using the proposed MBL model and cohesive zone models is currently being pursued by the authors. Moreover, the proposed MBL model can be employed to analyze the elastic–plastic crack-tip fields along a 3-D surface crack-front in FGMs, however, predominant plane-stress conditions near the free surface may limit the range of application of the MBL model.

Acknowledgements

This work was supported by the “Post-doctoral Fellowship Program” of Korea Science & Engineering Foundation (KOSEF) and the M.T. Geoffery Yeh Endowed Chair Fund at University of Illinois, Urbana-Champaign.

Appendix A. Calculation of SIF and T -stress based on interaction integral

The interaction integral method constitutes a post-processing step that utilizes the stresses, strains and displacements generated during the solution of a boundary-value problem. Here the numerically-calculated quantities are referred as *actual* fields. By superimposing *actual* fields with *auxiliary* fields corresponding to a second, arbitrary equilibrium state, fields for the *superimposed* state are obtained. For this superimposed state, domain integral at location s along the crack-front given by Shih et al. [35] becomes

$$\begin{aligned} \bar{J}^{(S)}(s) = & \int_V \left[\left(\sigma_{ij}^{(1)} + \sigma_{ij}^{(2)} \right) \left(u_{j,1}^{(1)} + u_{j,1}^{(2)} \right) - \frac{1}{2} \left(\sigma_{jk}^{(1)} + \sigma_{jk}^{(2)} \right) \left(\epsilon_{jk}^{(1)} + \epsilon_{jk}^{(2)} \right) \delta_{li} \right] q_{,i} dV \\ & + \int_V \left[\left(\sigma_{ij}^{(1)} + \sigma_{ij}^{(2)} \right) \left(u_{j,1}^{(1)} + u_{j,1}^{(2)} \right) - \frac{1}{2} \left(\sigma_{jk}^{(1)} + \sigma_{jk}^{(2)} \right) \left(\epsilon_{jk}^{(1)} + \epsilon_{jk}^{(2)} \right) \delta_{li} \right] ,_i q dV, \end{aligned} \quad (A1)$$

where σ_{ij} , u_i , and ϵ_{ij} denote the stresses, displacements and strains for the crack-front fields expressed in a local, orthogonal coordinate system at s on the curve front. Superscripts (1) and (2) indicate actual and auxiliary fields, respectively, and (S) denotes the superimposed state. V defines the volume centered about point s over which the analyst defined, weight function (q) has nonvanishing values and nonvanishing derivatives. Additional integrals for applied crack-face tractions are not shown. Eq. (A1) separates into three components:

$$\bar{J}^{(S)}(s) = \bar{J}^{(1)}(s) + \bar{J}^{(2)}(s) + \bar{I}(s), \quad (A2)$$

where $\bar{J}^{(S)}(s)$ is the domain integral for the superimposed state, $\bar{J}^{(1)}(s)$ is the domain integral for the actual state, $\bar{J}^{(2)}(s)$ is the domain integral for the auxiliary state, and $\bar{I}(s)$ is the domain form of the interaction integral, written as

$$\begin{aligned} \bar{I}(s) = & \int_V \left[\sigma_{ij}^{(1)} u_{j,1}^{(2)} + \sigma_{ij}^{(2)} u_{j,1}^{(1)} - \frac{1}{2} \left(\sigma_{jk}^{(1)} \epsilon_{jk}^{(2)} + \sigma_{jk}^{(2)} \epsilon_{jk}^{(1)} \right) \delta_{li} \right] q_{,i} dV \\ & + \int_V \left[\sigma_{ij}^{(1)} u_{j,1}^{(2)} + \sigma_{ij}^{(2)} u_{j,1}^{(1)} - \frac{1}{2} \left(\sigma_{jk}^{(1)} \epsilon_{jk}^{(2)} + \sigma_{jk}^{(2)} \epsilon_{jk}^{(1)} \right) \delta_{li} \right] ,_i q dV. \end{aligned} \quad (A3)$$

Auxiliary fields must satisfy equilibrium, compatibility, and constitutive relations at crack-front location s where the asymptotic functions maintain validity for both homogeneous and graded material [8]. For FGMs, this requires that material properties correspond to the crack-front location s , but over a finite domain of integration, material properties at element integration points can be significantly different from properties at the crack-front. To account for this discrepancy, Dolbow and Gosz [36] define strains according to

$$\epsilon_{ij}^{(2)} = S_{ijkl}(x)\sigma_{kl}^{(2)}, \quad (\text{A4})$$

where $S_{ijkl}(x)$ is the spatially-varying compliance tensor. Except at crack-front location s , Eq. (A4) violates strain–displacement compatibility. Also the following relationship enables us to simplify the expression of $\bar{I}(s)$:

$$\sigma_{ij,1}^{(1)}\epsilon_{ij}^{(2)} = C_{ijkl,1}(x)\epsilon_{kl}^{(1)}\epsilon_{ij}^{(2)} + \sigma_{ij}^{(2)}\epsilon_{kl,1}^{(1)}. \quad (\text{A5})$$

Consideration of this “incompatibility” and Eq. (A5) leads to the expression WARP3D employs to evaluate the interaction integral:

$$\bar{I}(s) = \int_V \left(\sigma_{ij}^{(1)} u_{j,1}^{(2)} + \sigma_{ij}^{(2)} u_{j,1}^{(1)} - \sigma_{jk}^{(1)} \epsilon_{jk}^{(2)} \delta_{li} \right) q_{,si} dV + \int_V \left[\sigma_{ij}^{(1)} \left(u_{j,1i}^{(2)} - \epsilon_{ij,1}^{(2)} \right) - C_{ijkl,1}(x) \epsilon_{kl}^{(1)} \epsilon_{ij}^{(2)} \right] q dV. \quad (\text{A6})$$

For homogeneous materials, the second integral in Eq. (A6) vanishes. Eq. (A6) is valid for quasi-static, isothermal, linear-elastic loading of FGMs in the absence of body forces. In this expression, auxiliary displacements are the only quantities that employ material properties corresponding to crack-front location, s . The compliance tensor for the FGM uses material properties at the location of the integration point. With $\bar{I}(s)$ calculated, the pointwise value for the interaction integral at location s along the 3-D crack front becomes:

$$I(s) = \frac{\bar{I}(s)}{\int_{L_c} q(s) ds}. \quad (\text{A7})$$

The energy release rate for the superimposed equilibrium state, in terms of the mixed-mode stress intensity factors for the actual and auxiliary fields, is

$$\begin{aligned} J^{(S)}(s) &= \frac{1}{E^*(s)} \left[\left(K_{\text{I}}^{(1)} + K_{\text{I}}^{(2)} \right)^2 + \left(K_{\text{II}}^{(1)} + K_{\text{II}}^{(2)} \right)^2 \right] + \frac{1 + \nu(s)}{E(s)} \left(K_{\text{III}}^{(1)} + K_{\text{III}}^{(2)} \right)^2 \\ &= J^{(1)}(s) + J^{(2)}(s) + I(s), \end{aligned} \quad (\text{A8})$$

where

$$I(s) = \frac{1}{E^*(s)} \left(2K_{\text{I}}^{(1)}K_{\text{I}}^{(2)} + 2K_{\text{II}}^{(1)}K_{\text{II}}^{(2)} \right) + \frac{1 + \nu(s)}{E(s)} \left(2K_{\text{III}}^{(1)}K_{\text{III}}^{(2)} \right). \quad (\text{A9})$$

For a plane-stress and plane-strain conditions, $E^*(s) = E(s)$ and $E^*(s) = E(s)/(1 - \nu(s)^2)$, respectively. Eqs. (A6)–(A8) provide the necessary relationship between the interaction integral and actual stress intensity factors. By alternately assigning a nonzero value to only one auxiliary stress intensity factor, Eq. (A8) yields

$$K_{\text{I}}(s) = \frac{E^*(s)}{2} I(s), \quad K_{\text{II}}(s) = \frac{E^*(s)}{2} I(s), \quad \text{and} \quad K_{\text{III}}(s) = \mu(s) I(s). \quad (\text{A10})$$

To calculate T -stresses, Cardew et al. [26] and Kfoury [37] consider a 2-D line integral analogous to the first integral in Eq. (A6):

$$I = \int_{\Gamma} \left[\sigma_{jk}^{(1)} \epsilon_{jk}^{(2)} \delta_{li} - \left(\sigma_{ij}^{(1)} u_{j,1}^{(2)} + \sigma_{ij}^{(2)} u_{j,1}^{(1)} \right) \right] n_i d\Gamma. \quad (\text{A11})$$

When the Williams’ solution including the nonsingular T -stress term defines the actual fields and auxiliary fields given by Michell [38] defines the auxiliary fields, Eq. (A11) yields the following relationship:

$$T_{11} = \frac{E^* I}{f}. \quad (\text{A12})$$

For WARP3D simulations of 2-D problems, Eqs. (A6) and (A7) yield a value for $I(s)$ that can be used in Eq. (A12) when actual fields are taken from the finite-element solution, and auxiliary fields follow Michell [38]. Values of T_{11} calculated in this manner are valid for simulations of 2-D problems with in-plane mode-I or mode-II loading.

Appendix B. Tamura–Tomota–Ozawa (TTO) model

The TTO model [34] couples the uniaxial stress, σ , and strain, ϵ , of a two-phase composite to the corresponding average uniaxial stresses and strains of the two constituent materials by

$$\sigma = V_1\sigma_1 + V_2\sigma_2, \quad \epsilon = V_1\epsilon_1 + V_2\epsilon_2, \quad (\text{B1})$$

where σ_i and ϵ_i ($i = 1, 2$) denote the average stresses and strains of the constituent phases, respectively, and V_i ($i = 1, 2$) define the volume fractions. The TTO model introduces an additional parameter, q ,

$$q = \frac{\sigma_1 - \sigma_2}{|\epsilon_1 - \epsilon_2|}, \quad 0 < q < \infty \quad (\text{B2})$$

to describe the ratio of stress-to-strain transfer. The value of q depends on the constituent material properties and the microstructural interaction within the composite. For example, $q \rightarrow \infty$ if the constituent elements deform identically in the loading direction, while $q = 0$ if the constituent elements experience the same stress level. In general, the constituent elements in a composite undergo neither equal strain nor equal stress due to the complicated microstructure (variations in particle shape, orientation, volume fraction, etc.). A nonzero, finite value of q reflects approximately those effects. For applications involving plastic deformation of ceramic/metal (brittle/ductile) composites, the TTO model assumes that the composite yields once the metal constituent yields. With these assumptions, the Young's modulus, E , and the yield stress, σ_Y , of the composite may be obtained as follows [34]:

$$E = \left[V_2 E_2 \frac{q + E_1}{q + E_2} + (1 - V_2) E_1 \right] / \left[V_2 \frac{q + E_1}{q + E_2} + (1 - V_2) \right], \quad (\text{B3})$$

$$\sigma_Y(V_2) = \sigma_0 \left[V_2 + \frac{q + E_2}{q + E_1} \frac{E_1}{E_2} (1 - V_2) \right], \quad (\text{B4})$$

where E_i ($i = 1, 2$) are Young's moduli of the constituent phases, and σ_0 denotes the yield stress of the metal (phase 2). The above equation indicates that the yield stress of the composite depends on the yield stress of the metal, the volume fraction of the metal, Young's moduli of the constituent phases, and the parameter q . Poisson's ratio, ν of the composite just follows a rule of mixtures in the TTO model:

$$\nu = V_1\nu_1 + V_2\nu_2, \quad (\text{B5})$$

where ν_i ($i = 1, 2$) are Poisson's ratios of the constituent phases. For an idealized bilinear model of metal yield and hardening, the TTO model predicts that the composite also follows a bilinear response, as adopted in the previous study on ceramic/metal FGMs [29,32,33]. For many structural metals, however, the simplistic bilinear model does not capture adequately the variation in strain hardening rate under increased plastic flow. Jin et al. [17] proposed to use a more descriptive power-law model for both the metal and the composite. Therefore, the stress–strain curves of the metal and composite beyond the yield points have the form

$$\epsilon_2 = \epsilon_0 \left(\frac{\sigma_2}{\sigma_0} \right)^{n_0}, \quad \sigma_2 \geq \sigma_0, \quad (\text{B6})$$

and

$$\epsilon = \epsilon_Y \left(\frac{\sigma}{\sigma_Y} \right)^n, \quad \sigma \geq \sigma_Y, \quad (\text{B7})$$

respectively, where $\epsilon_0 = \sigma_0/E_2$ and $\epsilon_Y = \sigma_Y/E$ are the yield strains of the metal and composite, respectively and n_0 and n are the hardening exponents of the metal and composite, respectively. The following parametric equations determine the stress–strain (σ – ϵ) curve for the composite [17]:

$$\begin{aligned} \frac{\epsilon}{\epsilon_Y} &= \frac{V_1 E}{q + E_1} \frac{\sigma_2}{\sigma_Y} + \frac{(q + V_2 E_1) E}{(q + E_1) E_2} \frac{\sigma_0}{\sigma_Y} \left(\frac{\sigma_2}{\sigma_0} \right)^{n_0}, \\ \frac{\sigma}{\sigma_Y} &= \frac{V_2 q + E_1}{q + E_1} \frac{\sigma_2}{\sigma_Y} + \frac{V_1 q E_1}{(q + E_1) E_2} \frac{\sigma_0}{\sigma_Y} \left(\frac{\sigma_2}{\sigma_0} \right)^{n_0}. \end{aligned} \quad (\text{B8})$$

The composite σ – ϵ curve determined from the above equations does not follow the power function (B7). A least squares method determines n to approximate (B8) by (B7).

The phenomenological parameter q influences the “shape” of the stress–strain curve. In an average sense, the value of q reflects the composition and the complex microscale interaction of the constituents in an FGM. In practice, q may be determined approximately by experimental calibration using tensile tests performed on monolithic composite specimens. For example, a value of $q = 4.5$ GPa was found to be appropriate for dual phase steels [34].

References

- [1] Larsson SG, Carlsson AJ. Influence of non-singular stress terms and specimen geometry on small-scale yielding at crack tips in elastic–plastic materials. *J Mech Phys Solids* 1973;21:263–77.
- [2] Bilby BA, Cardew GE, Goldthorpe MR, Howard IC. A finite element investigation of the effect of specimen geometry on the fields of stress and strain at the tip of stationary cracks. *Size Effect in Fracture, I Mech E, London*, 1986;37–46.
- [3] Betegon C, Hancock JW. Two-parameter characterization of elastic–plastic crack-tip fields. *J Appl Mech, Trans ASME* 1991;58:104–10.
- [4] Xia L, Shih CF. Ductile crack growth—I. A numerical study using computational cells with microstructurally-based length scales. *J Mech Phys Solids* 1995;43:233–59.
- [5] Williams ML. On the stress distribution at the base of stationary crack. *J Appl Mech, Trans ASME* 1957;24:109–14.
- [6] Paulino GH, Jin ZH, Dodds Jr RH. Failure of functionally graded materials. *Comprehensive structural integrity*, vol. 2. Elsevier Science; 2003. p. 607–44. Chapter 13.
- [7] Delale F, Erdogan F. The crack problem for a nonhomogeneous plane. *J Appl Mech, Trans ASME* 1983;50:609–14.
- [8] Eischen JW. Fracture of non-homogeneous materials. *Int J Fract* 1987;34:3–22.
- [9] Gu P, Asaro RJ. Crack deflection in functionally graded materials. *Int J Solids Struct* 1997;34:3085–98.
- [10] Marur PR, Tippur HV. Numerical analysis of crack-tip fields in functionally graded materials with a crack normal to the elastic gradient. *Int J Solids Struct* 2000;37:5353–70.
- [11] Anlas G, Lambros J, Santare MH. Dominance of asymptotic crack tip fields in elastic functionally graded materials. *Int J Fract* 2002;115:193–204.
- [12] Erdogan F. Fracture mechanics of functionally graded materials. *Compos Engng* 1995;5:753–70.
- [13] Eftis J, Subramonian N, Liebowitz H. Crack border stress and displacement equations revisited. *Engng Fract Mech* 1977;9:189–210.
- [14] Anderson TL. *Fracture mechanics: fundamentals and applications*. Boca Raton: CRC Press LLC; 1995.
- [15] Anlas G, Santare MH, Lambros J. Numerical calculation of stress intensity factors in functionally graded materials. *Int J Fract* 2000;104:131–43.
- [16] Kim JH, Paulino GH. Isoparametric graded finite elements for nonhomogeneous isotropic and orthotropic materials. *J Appl Mech, Trans ASME* 2002;69:502–14.
- [17] Jin ZH, Paulino GH, Dodds Jr RH. Cohesive fracture modeling of elastic–plastic crack growth in functionally graded materials. *Engng Fract Mech* 2003;70:1885–912.
- [18] Santare MH, Lambros J. Use of graded finite elements to model the behavior of nonhomogeneous materials. *J Appl Mech, Trans ASME* 2000;67:819–22.
- [19] Gullerud AS, Koppenhoefer KC, Roy YA, RoyChowdhury S, Walters M, Bichon B, et al. *WARP3D Release 15 Manual, Civil Engineering, Report No. UIUC-ENG-95-2012, University of Illinois at Urbana–Champaign, Urbana, IL*, 2004.
- [20] Yau JF, Wang SS, Corten HT. A mixed-mode crack analysis of isotropic solids using conservation laws of elasticity. *J Appl Mech, Trans ASME* 1980;47:335–41.
- [21] Nakamura T, Parks DM. Determination of elastic T-stress along three-dimensional crack fronts using an interaction integral. *Int J Solids Struct* 1992;29:1597–611.
- [22] Nakamura T, Parks DM. Three-dimensional stress field near the crack front of a thin elastic plate. *J Appl Mech, Trans ASME* 1988;55:805–13.
- [23] Walters MC, Paulino GH, Dodds Jr RH. Interaction-integral procedures for 3-D curved cracks including surface tractions. *Engng Fract Mech* 2005;72:1635–63.
- [24] Walters MC, Paulino GH, Dodds Jr RH. Computation of mixed-mode stress intensity factors for cracks in three-dimensional functionally-graded solids. *ASCE J Engng Mech*, in press.
- [25] Kim JH, Paulino GH. T-stress, mixed-mode stress intensity factors, and crack initiation angles in functionally graded materials: a unified approach using the interaction integral method. *Comp Meth Appl Mech Engng* 2003;192:1463–93.
- [26] Cardew GE, Goldthorpe MR, Howard IC, Kfoury AP. On the elastic T-term. *Fundamentals of deformation and fracture*. In: Bilby BA, Miller KJ, Willis JR, editors. *Eshelby Memorial Symp*. Sheffield: Cambridge University Press; 1985. p. 465–76.
- [27] Hill MR, Carpenter RD, Paulino GH, Munir ZA, Gibeling JC. Fracture testing of a layered functionally graded material. In: Salem JA, Quinn GD, Jenkins MG, editors. *Fracture resistance testing of monolithic and composite brittle materials ASTM STP1409*. West ConshohockenPA: American Society for Testing and Materials; 2002.
- [28] Nelson G, Ezis A. Functionally graded material (FGM) armor in the TiB/Ti system (U). *CERCOM Report, Vista, CA*, 1996.

- [29] Carpenter RD, Liang WW, Paulino GH, Gibeling JC, Munir ZA. Fracture testing and analysis of a layered functionally graded Ti/TiB beam in 3-point bending. *Mater Sci Forum* 1999;308–311:837–42.
- [30] Paulino GH, Carpenter RD, Liang WW, Munir ZA, Gibeling JC. Fracture testing and finite element modeling of pure titanium. *Engng Fract Mech* 2001;68:1417–32.
- [31] Kim JH, Paulino GH. An accurate scheme for mixed-mode fracture analysis of functionally graded materials using the interaction integral and micromechanics models. *Int J Numer Meth Engng* 2003;58:1457–97.
- [32] Williamson RL, Rabin BH, Drake JT. Finite element analysis of thermal residual stresses at graded ceramic–metal interfaces, Part I: Model description and geometrical effects. *J Appl Phys* 1993;74:1310–20.
- [33] Giannakopoulos AE, Suresh S, Finot M, Olsson M. Elastoplastic analysis of thermal cycling: layered materials with compositional gradients. *Acta Metall Mater* 1995;43:1335–54.
- [34] Tamura I, Tomota Y, Ozawa H. Strength and ductility of Fe–Ni–C alloys composed of austenite and martensite with various strength. *Proceedings of the third international conference on strength of metals and alloys, vol. 1*. Cambridge: Institute of Metals; 1973. p. 611–5.
- [35] Shih CF, Moran B, Nakamura T. Energy release rate along a three-dimensional crack front in a thermally stressed body. *Int J Fract* 1986;30:79–102.
- [36] Dolbow J, Gosz M. On the computation of mixed-mode stress intensity factors in functionally graded materials. *Int J Solids Struct* 2002;39:2557–74.
- [37] Kfourfi AP. Some evaluations of the elastic T-term using Eshelby's method. *Int J Fract* 1986;30:301–15.
- [38] Michell JH. Elementary distributions of plane stress. *Proceedings of the London Mathematical Society* 1900;32:35–61.